A CASPT2 Theoretical Study of the Kinetics of the 2-, 3-, and 4-Methylbenzylperoxy Radical Isomerization

Sébastien Canneaux,* Florent Louis, Marc Ribaucour,* Abderrahman El Bakali, and Jean-François Pauwels

PhysicoChimie des Processus de Combustion et de l'Atmosphère (PC2A) UMR CNRS 8522, FR CNRS 2416 Centre d'Etudes et de Recherche Lasers et Applications (CERLA), Université des Sciences et Technologies de Lille, 59655 Villeneuve d'Ascq Cedex, France

Received: December 17, 2008; Revised Manuscript Received: January 19, 2009

The rate constants of the 2-, 3-, and 4-methylbenzylperoxy isomerization reactions have been computed using the elaborated CASPT2 method. Geometry optimizations and vibrational frequency calculations are performed with two methods (B3LYP and MPW1K) combined with the cc-pVDZ and 6-31+G(d,p) basis sets, respectively. Single-point energy calculations are performed at the CASPT2/ANO-L-VDZP//B3LYP/cc-pVDZ level of theory as recommended by Canneaux et al. (*J. Phys. Chem. A* **2008**, *112*, 6045). Canonical transition-state theory with a simple Wigner tunneling correction is used to predict the high-pressure limit rate constants as a function of temperature. They are given by the following relations for the 2-, 3-, and 4-methylbenzylperoxy (MBP) (1,3s) isomerizations and for the 2-methylbenzylperoxy (1,6p) isomerization, respectively: $k_{2\text{-MBP(1,3s)}}(600-2000\ \text{K})\ (\text{in s}^{-1}) = (3.33 \times 10^{10})T^{0.79} \exp((-142.6\ \text{in kJ mol}^{-1})/RT)$; $k_{3\text{-MBP(1,3s)}}(600-2000\ \text{K})\ (\text{in s}^{-1}) = (0.74 \times 10^{10})T^{0.79} \exp((-130.7\ \text{in kJ mol}^{-1})/RT)$; $k_{4\text{-MBP(1,3s)}}(600-2000\ \text{K})\ (\text{in s}^{-1}) = (1.12 \times 10^{10})T^{0.79} \exp((-133.6\ \text{in kJ mol}^{-1})/RT)$; $k_{2\text{-MBP(1,6p)}}(600-2000\ \text{K})\ (\text{in s}^{-1}) = (5.10 \times 10^{8})T^{0.85} \exp((-87.1\ \text{in kJ mol}^{-1})/RT)$. These parameters can be used in the thermokinetic models involving aromatic compounds at high pressure. In the case of the 2-methylbenzylperoxy radical, the (1,6p) H-atom transfer reaction is consistently the most important channel over the studied temperature range, and the (1,3s) H-atom transfer reaction is not energetically favored.

I. Introduction

One of the main research objectives of our laboratory is to develop detailed thermokinetic combustion models valid in a wide range of operating conditions: from low to high pressures (subatmospheric pressure to a dozen of bars) and from low to high temperatures (600−2000 K). The building of these models is not easy due to the considerable lack of thermochemical and kinetic data, especially in the case of aromatic compounds.

At low temperature, the internal H-atom transfer reactions of peroxy radicals are rate-determinant steps in the oxidation process of many fuels,[1] but practically no experimental kinetic parameters are available for these reactions. The reason is that on one hand they are difficult to isolate and on the other hand they lead to the formation of many isomers. The use of quantum chemistry methods, statistical thermodynamics, and canonical transition-state theory is a valuable solution to fill in the lack of experimental kinetic data. This approach has already been adopted with success in our laboratory to determine the high-pressure limit rate constant of the (1,3s) internal H-atom transfer reaction of benzylperoxy radical.[2] In this previous article, a methodological study using 54 different levels of theory has been carried out and has shown that standard theoretical methods are not adequate to obtain a quantitative rate constant for the considered reaction: the use of the elaborated CASPT2 method is needed. This methodological study has allowed the determination of the appropriate level of theory to obtain an excellent agreement between the calculated value and the only single experimental value reported by Ellis et al.[3] at 773 K. The CASPT2/ANO-L-VDZP//B3LYP/cc-pVDZ level of theory has been identified as the most appropriate one leading to a ratio of the calculated rate constant over the experimental one equal to 0.9. In the present article, which is part of a series devoted to the generation of kinetic data for alkyl side chain aromatic compounds, the CASPT2/ANO-L-VDZP//B3LYP/cc-pVDZ level of theory is used to calculate the rate constants of internal H-atom transfer reactions of 2-, 3-, and 4-methylbenzylperoxy radicals (*o*-, *m*-, and *p*-xylylperoxy radicals). Table 1 gathers the structures and names of some species mentioned in the text as well as their common and systematic names.

Useful properties of aromatic hydrocarbons and their negative impact on environment and health have been mentioned in our recent articles[2,4] and will not be recalled here. In order to reduce the emission of pollutants and toxic compounds, engines builders perform combustion modeling studies in engine. This numerical work needs thermokinetic models for the combustion of surrogate fuels including representative fuels of each family of compounds present in commercial fuels. The family of alkylbenzenes is present in gasoline, diesel fuel, and kerosene. The percentages in weight of this family in a European gasoline, a diesel fuel, and a kerosene are 32, 9, and 24%, respectively.[5] Xylenes are good candidates to represent this family in a surrogate fuel. Their percentages in mass in a European gasoline are 3.06, 5.70, and 1.96% for *o*-, *m*-, and *p*-xylene, respectively.[5] Xylenes exhibit good combustion properties for use in spark-ignited engines due to their high research octane numbers[6,7] (113.0 for *o*-xylene, 117.5 for *m*-xylene, and 116.4 for *p*-xylene).

Few experimental and modeling studies on oxidation of *o*-, *m*-, and *p*-xylene have been conducted at temperatures of interest

* To whom correspondence should be addressed. Fax: (33)3-20436977. E-mail: sebastien.canneaux@univ-lille1.fr (S.C); marc.ribaucour@univ-lille1.fr (M.R.).

10.1021/jp811137d CCC: $40.75
Published on Web 02/25/2009

TABLE 1: Structures and Names for Some Species Mentioned in the Text

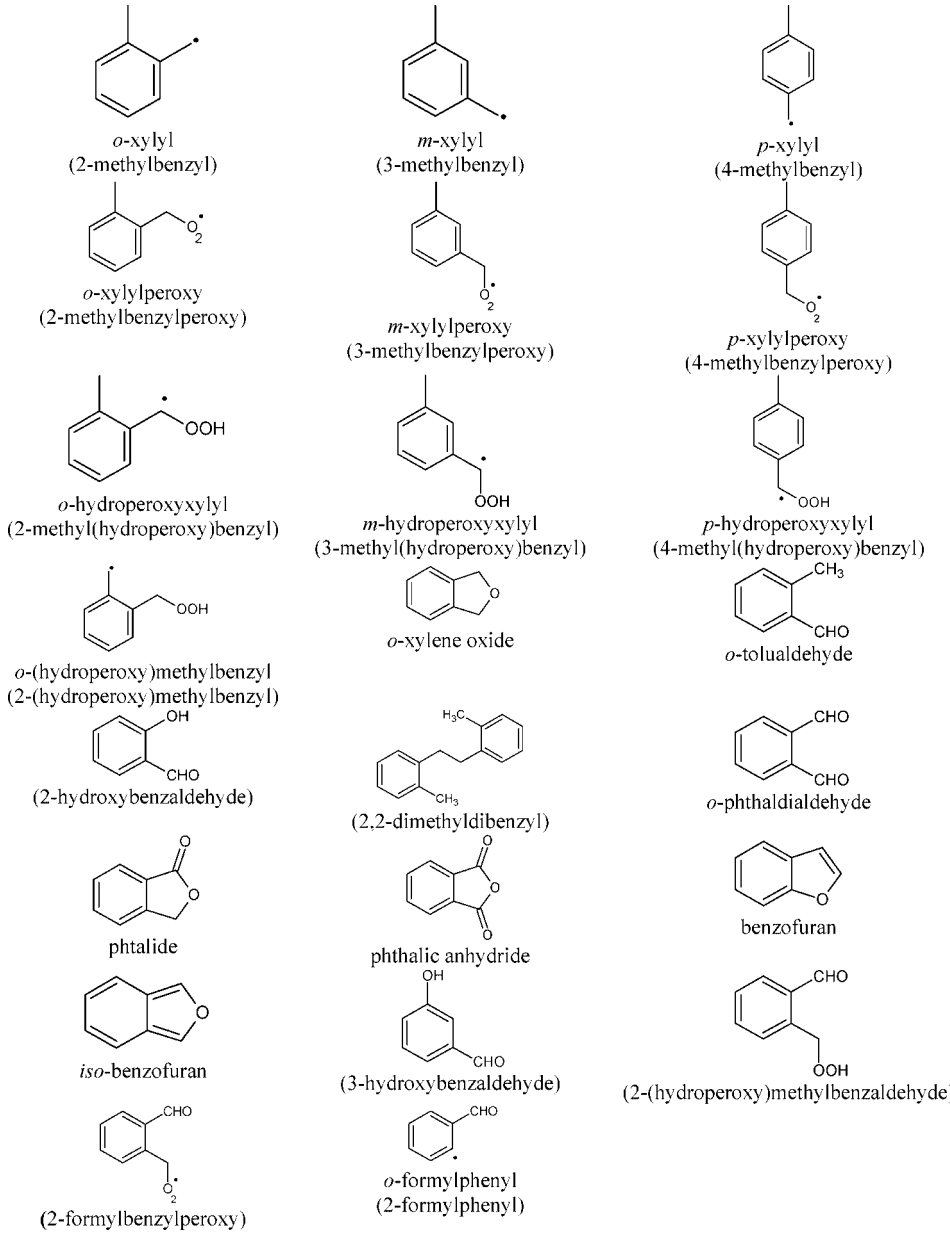

in combustion. The most recent of them are high-temperature (T > 900 K) studies.[8−14] Emdee et al.[8,9] have studied the oxidation of the three xylene isomers in an atmospheric flow reactor, with a high dilution by nitrogen (mole fraction of N_2 > 0.97), from 1093 to 1199 K, and for equivalence ratios (ϕ) from 0.47 to 1.7. The major aromatic intermediates which have been analyzed during the oxidation of *o*-xylene include benzene, toluene, *o*-tolualdehyde, *o*-methylstyrene, benzaldehyde, and styrene. In the case of *m*- and *p*-xylenes, the major aromatic intermediates which have been detected for both isomers are benzene, toluene, tolualdehyde, ethyltoluene, benzaldehyde, ethylbenzene, styrene, methylbenzyl alcohol, methylstyrene, and 1,2-ditolylethane. Reaction schemes for the high-temperature oxidation of the three xylenes have been proposed. Gregory and Jackson[10]have investigated the combustion chemistry leading to the formation of aromatic hydrocarbons from deuterium-labeled isomeric xylenes in the exhaust of a single-cylinder spark-ignition engine under stoichiometric conditions. The major aromatic hydrocarbons produced by the oxidation of each xylene were benzene, toluene, ethylbenzene, styrene, and ethyltoluene. Gaïl and Dagaut[13] have studied the oxidation of *p*-xylene in a jet-stirred reactor, at 1 atm, under high dilution conditions (mole fraction of N_2 > 0.97), over the temperature range 900−1300 K, and for equivalence ratios from 0.5 to 1.5. The mole fraction profiles of the reactants, stable intermediates, and final products have been measured versus temperature by sonic probe sampling and gas chromatography analyses. The experiments have been successfully modeled using a detailed thermokinetic model including 160 species and 1175 reactions. The proposed model has been also successfully tested against the ignition delays of *p*-xylene/O_2/Ar mixtures measured in a shock tube[12] and against some species mole fraction profiles obtained by Dupont[11] in a low-pressure $CH_4/O_2/N_2$ flame doped with *p*-xylene. Battin-Leclerc et al.[14] have conducted an experimental and modeling study of the oxidation of xylene isomers. Ignition delay times of xylene/O_2/Ar mixtures from 3 to 800 μs have been measured in a shock tube at pressures from 6.7 to 9 bar, between 1330 and 1800 K, for three equivalence ratios (ϕ = 0.5, 1, and 2), for two mole fractions of xylene (0.375 and 0.625), and under high dilution (mole fraction of Ar > 0.91). A detailed thermo-

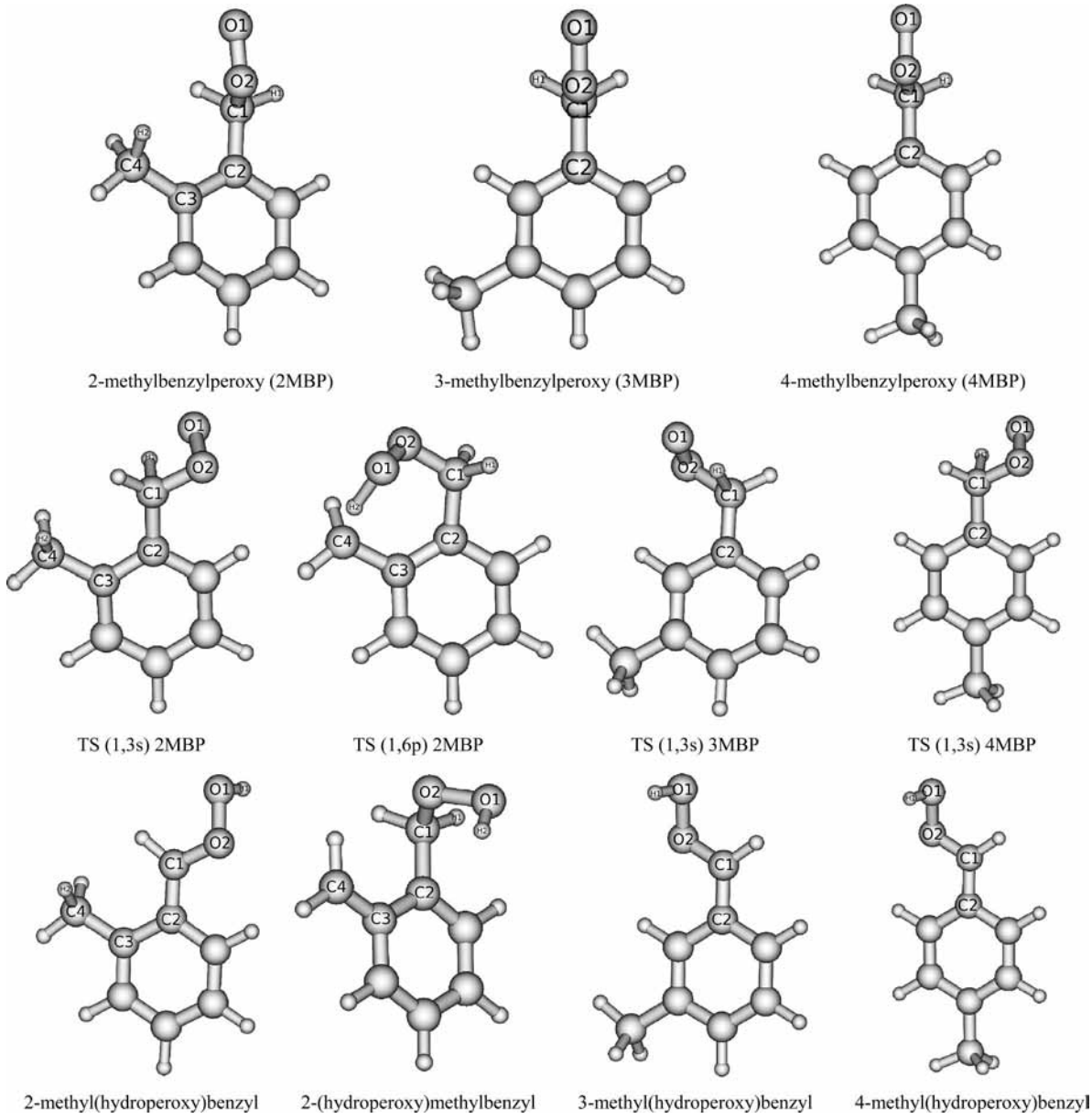

Figure 1. Structure and atom numbering of the different species involved in the reaction.

kinetic model (190 species and 1290 reactions) has been proposed. It reproduces well the ignition delay times measured in this study as well as mole fraction profiles of reactants and main intermediates versus residence time from the flow reactor studies of Emdee et al.[8,9] Flux and sensitivity analyses have allowed an explanation of the differences of reactivity observed between the three isomers.

Low-temperature ($T < 900$ K) studies on the oxidation of xylenes are sparse, and most of them have been carried out in the sixties. Loftus and Satterfield[15] have studied the partial oxidation of a lean ($\phi = 0.5$) *o*-xylene/air mixture in a flow reactor at 1 atm from 728 to 798 K, at a residence time of 6−7 s. Eleven aromatic oxidation products have been identified by gas chromatography, infrared spectroscopy, and nuclear magnetic resonance spectroscopy. *o*-Xylene oxide (phtalan) followed by *o*-tolualdehyde are the major oxidation products. *o*-Xylene oxide and 2,2-dimethyldibenzyl are formed early, whereas *o*-tolualdehyde is produced by subsequent reactions. A reaction scheme has been suggested to account for the formation of the following aromatic oxidation products: *o*-xylene oxide, *o*-tolualdehyde, *o*-phthaldialdehyde, phthalide, phthalic anhydride, benzaldehyde, and benzene. This scheme involves the formation of *o*-xylyl radical $Ph(CH_2°)(CH_3)$ (Ph stands for the aromatic nucleus) by hydrogen abstraction from *o*-xylene by O_2 and OH radical. *o*-Xylylperoxy radical $Ph(CH_2OO°)(CH_3)$ is then produced by addition of O_2 to *o*-xylyl radical. Two internal H-atom transfer reactions are proposed to explain the formation of *o*-xylene oxide and *o*-tolualdehyde from *o*-xylylperoxy radical. The (1,6p) H-atom transfer reaction of *o*-xylylperoxy radical yields the $Ph(CH_2OOH)(CH_2°)$ radical. Subsequent cleavage of the weak O−O bond coupled with a cyclization leads to the formation of *o*-xylene oxide. The (1,3s) H-atom transfer reaction of *o*-xylylperoxy radical yields the $Ph(C°HOOH)(CH_3)$ radical. Subsequent cleavage of the weak O−O bond leads to the formation of *o*-tolualdehyde. Barnard and Sankey[16,17] have studied the slow oxidation of the three xylene isomers in a static reactor, from 733 to 785 K, at pressures below 250 Torr, and for rich (ϕ ranging from 2.63 to 5.2) fuel/O_2 mixtures. *m*-Xylene and *p*-xylene have shown a similar reactivity. *o*-Xylene has exhibited a higher reactivity toward molecular oxygen than the other isomers: under identical conditions, its maximum reaction rate was about 10 times higher than that of *m*- and *p*-xylenes.

Oxidation products have been analyzed by gas chromatography. Aromatic oxidation products of *m*- and *p*-xylenes are *m*- and *p*-tolualdehydes, respectively, as well as toluene, benzene, and benzaldehyde. Aromatic oxidation products of *o*-xylene are *o*-xylene oxide, *o*-tolualdehyde, benzofuran, and benzaldehyde. A reaction scheme involving a (1,6p) internal H-atom transfer reaction of *o*-xylylperoxy radical has been proposed to explain the formation of *o*-xylene oxide. Roubaud et al.[18] have performed an autoignition study of stoichiometric fuel/O_2/inert mixture in a rapid compression machine, at core gas temperatures ranging from 600 to 900 K and pressures up to 25 bar after compression, and at two dilutions: O_2/inert = 0.27 (dilution of air) and O_2/inert = 0.37. The autoignition features of 11 alkylbenzenes including the three xylene isomers have been compared in this study. The fuels have been classified into two groups: the first one includes fuels that ignite only above 16 bar at temperatures near 900 K. The second one includes fuels that may ignite below 16 bar. *m*-Xylene and *p*-xylene belong to the first group, whereas *o*-xylene belongs to the second group. Thus *o*-xylene is more reactive than the two other isomers. The autoignition delay times of stoichiometric *o*-xylene/O_2/inert mixtures (at a dilution O_2/inert = 0.37) have been measured between 600 and 900 K, and the following characteristics have been observed: a two-stage autoignition at temperature below 700 K, a one-stage autoignition at higher temperatures, and a slight negative temperature coefficient between 720 and 780 K. In a second study, Roubaud et al.[19] have measured the oxidation products of *o*-xylene formed at a time after the first stage and before the second stage of the autoignition under the following conditions: 15.6 bar, 704 K, stoichiometric fuel/O_2/inert mixture, dilution O_2/inert = 0.37. The consumption of *o*-xylene was ~10% at this time. The amounts of product have been expressed in terms of carbon selectivities, i.e., in number of carbon atoms in the species normalized to 100 carbon atoms of fuel consumed. The products exhibiting the highest selectivities are, in decreasing order, 2-hydroxybenzaldehyde (~14%), *o*-xylene oxide (~13%), and 2-methylbenzaldehyde (*o*-tolualdehyde) (~9%). Toluene, isobenzofuran, 3-hydroxybenzaldehyde, *o*-phthaldialdehyde, and phthalide are among the minor aromatic oxidation products. The formation of the main oxidation products is explained by a low-temperature oxidation scheme involving the formation of the *o*-xylylperoxy radical $Ph(CH_2OO°)(CH_3)$ by addition of molecular oxygen to *o*-xylyl radical. Then, two internal H-atom transfer pathways of *o*-xylylperoxy radical are considered: a (1,6p) one yielding the radical $Ph(CH_2OOH)(CH_2°)$ and a (1,3s) one yielding the radical $Ph(C°HOOH)(CH_3)$. The radical $Ph(CH_2OOH)(CH_2°)$ produces *o*-xylene oxide after the breaking of the weak O−O bond with removal of an OH radical and a cyclization. The radical $Ph(C°HOOH)(CH_3)$ forms *o*-tolualdehyde after breaking of the O−O bond with removal of an OH radical and the formation of a C═O bond. To explain the formation of 2-hydroxybenzaldehyde, the following reaction sequence is suggested. The radical $Ph(CH_2OOH)(CH_2°)$ undergoes an O_2 addition followed by an internal H-atom transfer reaction to form the radical $Ph(C°HOOH)(CH_2OOH)$. This radical produces an oxohydroperoxide $Ph(CHO)(CH_2OOH)$ and an OH radical through the breaking of the weak O−O bond. Then, the oxohydroperoxide undergoes the breaking of the weak O−O bond to produce the radical $Ph(CHO)(CH_2O°)$ and an OH radical. This step is a branching pathway postulated in the low-temperature oxidation schemes of many fuels. Then, the radical $Ph(CHO)(CH_2O°)$ produces methanal and the *o*-formylphenyl radical °Ph-CHO by breaking of the C−C bond between the fragment $CH_2O°$ and the aromatic nucleus. Finally, this latter radical adds an OH radical to produce 2-hydroxybenzaldehyde.

The bibliographic synthesis of low-temperature studies on oxidation of xylene isomers shows the importance of the internal H-atom transfer pathways of methylbenzylperoxy radicals. The (1,6p) internal H-atom transfer reaction of 2-methylbenzylperoxy radical is postulated to explain the formation of *o*-xylene oxide, whereas (1,3s) internal H-atom transfer reactions of 2-, 3-, and 4-methylbenzylperoxy may be implicated in the formation of *o*-, *m*-, and *p*-tolualdehyde. In the case of the 2-methylbenzylperoxy radical, there could be a competition between the (1,6p) and (1,3s) transfer reactions. To our knowledge no experimental or calculated rate constant values are available for these aforementioned reactions. Thus a determination of the rate constants of these reactions is of high interest because it will allow us to incorporate them in a low-temperature oxidation model of xylene isomers. The aim of this article is to calculate accurate values of these rate constants using a highly correlated level of theory, statistical thermodynamics, and canonical transition-state theory.

Few theoretical studies have been carried out on the (1,3s) isomerizations of the alkylperoxy[20−24] and arylperoxy[2,25,26] radicals. More detailed discussion can be found in our previous article.[2] Concerning the (1,6p) isomerizations, only three previous studies have been reported in the literature concerning the butylperoxy[24,27] and pentylperoxy[20] radicals. Jungkamp et al.[27] worked on the atmospheric oxidation mechanism of *n*-butane. Part of this study concerned the (1,6p) isomerization of the butylperoxy radical for which the reaction barrier was 106.3 kJ mol^{-1} at the CBS-lq//B3LYP/6-31G(d,p) level of theory. Zhu et al.[24] performed theoretical calculations at the CBS-QB3 level of theory on the kinetics of the intramolecular hydrogen shift reactions of the butylperoxy radical. The energy barrier of the (1,6p) isomerization was estimated at 0 K to 94.6 kJ mol^{-1}. Chan et al.[20] performed BHandHLYP/6-311G(d,p) calculations estimating the activation energies and pre-exponential factors for a series of intramolecular hydrogen-atom abstraction reactions in alkylperoxy radicals containing up to five carbons. In particular, the calculated activation energy was about 125.1 kJ mol^{-1} for the (1,6p) isomerization reaction of the pentylperoxy radical.[20]

In this work, highly correlated quantum chemical calculations were performed in order to directly compute the barrier for the (1,3s) and (1,6p) isomerizations without any energy adjustments. The energetics of the reactant and the transition state (TS) was used together with transition-state theory (TST) calculations to compute the rate constants in the temperature range 600−2000 K. To our knowledge, this is the first time that the temperature dependence of the rate constant for the 2-, 3-, and 4-methylbenzylperoxy radical isomerizations has been computed at a highly correlated level of theory.

This article is organized as follows. Computational methods are reported in Section II, while the results are presented and discussed in Section III.

II. Computational Methods

Theoretical calculations were performed using the GAUSSIAN03[28] and MOLCAS 6.0[29] software packages. Reactants (2-, 3-, and 4-methylbenzylperoxy radicals) and TS structures were fully optimized at HF-DFT (B3LYP)[30,31] and MPW1K[32] levels of theory using, respectively, the Pople-style 6-31+G(d,p) basis set[33] and the Dunning's correlation consistent double-ζ plus polarization cc-pVDZ[34] basis set. Product geometries were fully optimized at the MPW1K/6-31+G(d,p) (2-, 3-, and 4-methyl-

(hydroperoxy)benzyl and 2-(hydroperoxy)methylbenzyl radicals) and B3LYP/cc-pVDZ (2-(hydroperoxy)methylbenzyl radical) levels of theory. All TSs have been characterized by one imaginary frequency (first-order saddle points) on the potential energy surface. Special care was taken to determine minimum energy pathways, performing intrinsic reaction coordinate (IRC) analyses[35] using all levels of theory, in order to confirm that a specific TS connects the different local minima. Vibrational frequencies were determined within the harmonic approximation at the same level of theory as for geometries. For the reactants and TS structures, single-point energy calculations were carried out on B3LYP/cc-pVDZ geometries at the CASPT2[36−39] level of theory with the ANO-L-VDZP[40] basis set.

It has been shown previously on the benzylperoxy radical isomerization[2] that it was necessary to obtain energy differences between the TS and the reactant at the CASPT2/ANO-L-VDZP//B3LYP/cc-pVDZ level of theory, particularly to carry out rate constant calculations through TST at a later stage. The CASPT2 method was carried out to incorporate both dynamic and nondynamic correlation effects on the relative energy ordering of the calculated stationary points. The CASPT2 approach is based on a second-order perturbation treatment where the CASSCF wave function is taken as the reference function. In this study, single-point CASPT2/CAS(3,3) calculations were obtained using again the ANO-L-VDZP basis set on the optimized geometries and excluding inner shells and corresponding virtual counterparts from the perturbation calculation. For the abstraction mechanism, the active space (3, 3) that best describes the C−H bond breaking and O−H bond forming includes the σ_{C-H} bonding molecular orbital (MO) with the associated σ^*_{C-H} antibonding MO and the single-electron MO.

Canonical TST[41] was used to predict the temperature dependence of the rate constants. Accordingly, the high-pressure limit rate constants, $k(T)$, were computed using the following expression

$$k(T) = \Gamma(T) \times \frac{k_B T}{h} \times \frac{Q_{TS}(T)}{Q_{\text{methylbenzylperoxyradical}}(T)} \times \exp\left(-\frac{E_0}{k_B T}\right) \quad \text{(II-1)}$$

where $\Gamma(T)$ indicates the transmission coefficient used for the tunneling correction at temperature T, and the terms $Q_{TS}(T)$ and $Q_{\text{methylbenzylperoxy radical}}(T)$ are the total partition functions for the TS and the methylbenzylperoxy radical at the temperature T. In eq II-1, the vibrationally adiabatic barrier height, E_0, is computed as the energy difference between the TS and the reactant, including zero-point energy corrections. k_B is Boltzman's constant, and h is Planck's constant.

The calculation of the reaction rate constants using the TST formulation given by eq II-1 requires the proper computation of the partition functions of the reactant and the TSs. The total partition function $Q^X(T)$ of a species X can be cast in terms of the translational $Q_T^X(T)$, electronic $Q_e^X(T)$, rotational $Q_R^X(T)$, and vibrational $Q_V^X(T)$ partition functions:

$$Q^X(T) = Q_T^X(T) Q_e^X(T) Q_R^X(T) Q_V^X(T) \quad \text{(II-2)}$$

In this work, we adopt the simple and computationally inexpensive Wigner method[42] in the calculation of all tunneling corrections for the reactions reported here

$$\Gamma(T) = 1 + \frac{1}{24}\left(\frac{h\nu^{\neq}}{k_B T}\right)^2 \quad \text{(II-3)}$$

where $\nu^{\neq}$ is the imaginary frequency at the saddle point. This choice seems to be appropriate for the tunneling corrections applied to rate constants at typical incineration/combustion temperatures (600−2000 K) for which the values of transmission coefficients $\Gamma(T)$ are small to moderate (≤ 2).[24,43] More sophisticated and computationally demanding algorithms such as the ones developed by Truhlar et al.[44] and Miller et al.[45] should be used if the transmission coefficients are much higher than the ones computed in this study. The rate constant calculations were performed over the temperature range of interest using the KISTHEP software.[46]

III. Results and Discussion

1. Geometric Parameters and Vibrational Frequencies. ***Geometric Parameters.*** Figure 1 shows the structures and atom numbering of the reactants (2-, 3-, and 4-methylbenzylperoxy radicals), the (1,3s) and (1,6p) isomerization TSs, and the products (2-, 3-, and 4-methyl(hydroperoxy)benzyl and 2-(hydroperoxy)methylbenzyl radicals). Table 2 gathers the selected bond lengths calculated at the two levels of theory. More detailed information regarding optimized Cartesian coordinates for these species is presented in Tables 1S−11S of the Supporting Information.

2-, 3-, and 4-Methylbenzylperoxy Radicals. The global minima for the 3- and 4-methylbenzylperoxy radicals are found at the B3LYP and MPW1K levels of theory to be in a conformation in which the dihedral angles $C_3C_2C_1O_2$ and $C_2C_1O_2O_1$ are equal to about −90° and 180°, respectively. The same results were obtained for the benzylperoxy radical by Garcia et al.[47] using the UHF/6-31G(d,p) and UHF/6-31+G(d,p) levels of theory and by Canneaux et al.[2] using 18 different geometry levels (B3LYP, MPW1K, and MP2 methods combined with six basis sets). The lowest energy conformer of the 2-methylbenzylperoxy radical is found to be at the two levels of theory in a slightly different conformation than those obtained for the 3-, and 4-methylbenzylperoxy radicals ($C_3C_2C_1O_2$ and $C_2C_1O_2O_1$ are equal to about −73° and 172°, respectively). This change in the structure can be explained with a more favored position in which hydrogen intramolecular bonding exists between the H_2 and O_2 atoms (in Figure 1). The hydrogen bond lengths $H_2\cdots O_2$ estimated at the B3LYP/cc-pVDZ and MPW1K/6-31+G(d,p) levels of theory are 2.619 and 2.655 Å, respectively.

It can be observed that the calculated geometric parameters for all methylbenzylperoxy radicals do not vary a lot as a function of the level of theory. For example, the O_1O_2 bond lengths estimated at the B3LYP/cc-pVDZ and MPW1K/6-31+G(d,p) levels of theory are 1.316 and 1.292 Å, respectively. The O_1O_2 and O_2C_1 key bond lengths in B3LYP geometries are slightly longer than those in MPW1K geometries. A similar but no so marked trend is observed for the C_1C_2, C_1H_1, C_4H_2, and C_4C_3 bond lengths. All the optimized geometric parameters are consistent with the ones reported for the benzylperoxy radical by Garcia et al.,[47] Murakami et al.,[26] and Canneaux et al.[2]

Transition States. For both (1,3s) and (1,6p) isomerizations, the unpaired electron on the OO σ-bond attacks one of the CH σ-bonds of the methyl fragment. The two electrons in the CH bond become unpaired, and one of these pairs with the peroxy function electron to form the OH bond in the corresponding product.

(1,3s) Transition States. The TS for isomerization of methylbenzylperoxy to methyl(hydroperoxy)benzyl radical is a four-

TABLE 2: Selected Bond Lengths in Angstroms for the Reactive Species Involved in the Isomerization Reactions[a]

		2-methylbenzylperoxy (1,3s) isomerization		2-methylbenzylperoxy (1,6p) isomerization		3-methylbenzylperoxy (1,3s) isomerization		4-methylbenzylperoxy (1,3s) isomerization	
		B3LYP cc-pVDZ	MPW1K 6-31+G(d,p)	B3LYP cc-pVDZ	MPW1K 6-31+G(d,p)	B3LYP cc-pVDZ	MPW1K 6-31+G(d,p)	B3LYP cc-pVDZ	MPW1K 6-31+G(d,p)
O_1O_2	R	1.316	1.292	1.316	1.292	1.315	1.292	1.315	1.292
	TS	*1.488*	*1.444*	*1.403*	*1.369*	*1.490*	*1.445*	*1.490*	*1.445*
	P	–	1.408	1.448	1.406	–	1.411	–	1.412
O_2C_1	R	1.477	1.446	1.477	1.446	1.477	1.446	1.478	1.446
	TS	*1.392*	*1.377*	*1.427*	*1.406*	*1.390*	*1.376*	*1.390*	*1.376*
	P	–	1.354	1.430	1.411	–	1.352	–	1.352
C_1C_2	R	1.500	1.492	1.500	1.492	1.496	1.491	1.498	1.490
	T	*1.470*	*1.462*	*1.521*	*1.509*	*1.470*	*1.462*	*1.469*	*1.460*
	P	–	1.402	1.511	1.499	–	1.402	–	1.402
H_1O_1	R	2.594	2.543			2.520	2.488	2.511	2.490
	TS	*1.337*	*1.307*			*1.337*	*1.306*	*1.339*	*1.308*
	P	–	0.960			–	0.960	–	0.960
C_1H_1	R	1.099	1.086			1.100	1.087	1.100	1.087
	TS	*1.304*	*1.295*			*1.303*	*1.294*	*1.302*	*1.293*
	P	–	2.710			–	2.683	–	2.672
H_2O_1	R			3.347	3.396				
	TS			*1.354*	*1.204*				
	P			0.976	0.960				
C_4H_2	R			1.101	1.088				
	TS			*1.354*	*1.312*				
	P			3.622	3.693				
C_4C_3	R			1.510	1.499				
	TS			*1.467*	*1.466*				
	P			1.409	1.402				

[a] R, TS, and P are, respectively, the reactant, the transition state, and the product of the reaction under study.

membered ring. The O_1O_2 bond length in the transition state is longer than the O_1O_2 bond length in the methylbenzylperoxy radical, but the H_1O_1 bond in TS is longer than the H_1O_1 bond in the methyl(hydroperoxy)benzyl radical. The peroxy function approach is calculated to occur nearly in the plane containing the $C_1H_1O_1O_2$ atoms. Structural parameters depend slightly on the level of theory.

(1,6p) Transition State. The TS for isomerization of 2-methylbenzylperoxy to 2-(hydroperoxy)methylbenzyl radical is a six-membered ring. The O_1O_2 bond length in the transition state is longer than the O_1O_2 bond length in the 2-methylbenzylperoxy radical, but the H_2O_1 bond in TS is shorter than the H_2O_1 bond in the 2-(hydroperoxy)methylbenzyl radical. The peroxy function approach is calculated to occur nearly in the two planes corresponding to the dihedral angle $C_1O_2O_1H_2$. Structural parameters depend slightly on the level of theory with the exception of the O_2H_1 bond length (1.354 and 1.204 Å using B3LYP/cc-pVDZ and MPW1K/6-31+G(d,p) levels, respectively). Application of diffuse functions tends to make this transition structure slightly more product-like. In the case of aliphatic compounds, the calculated O_2H_1 bond lengths were 1.140 Å (B3LYP/6-31G(d,p)) and 1.164 Å (BHandHLYP/6-311G(d,p)) for the (1,6p) transition states involved in the butylperoxy[27] and pentylperoxy[20] radical isomerization. The aromatic ring tends to strengthen the O_2H_1 bond length which takes place in the reaction coordinate.

2-, 3-, and 4-Methyl(hydroperoxy)benzyl Radicals. The global minimum is found with the MPW1K method in a conformation allowing the intramolecular interaction between the oxygen atom and the nearest hydrogen atom in the ring. Geometry optimizations at the B3LYP levels predict the absence of this stationary point on the potential energy surface. Similar results have been observed for the (hydroperoxy)benzyl radical[2,26] and for some alkylperoxy radicals.[21−24] The B3LYP method seems not to be adequate to obtain optimized $R\dot{C}HO_2H$ structures as discussed in our previous paper.[2] Structural parameters depend slightly on the position of the methyl group on the ring.

2-(Hydroperoxy)methylbenzyl Radical. The global minimum is found with both B3LYP and MPW1K methods. Calculated geometric parameters do not vary a lot as a function of the level of theory. The unpaired electron is located on the C_4 atom. The C_4C_3 bond (about 1.40 Å) acts indeed as a double bond because of the delocalized electron.

Vibrational Frequencies. Unscaled vibrational frequencies for these species are presented in Tables 12S−14S of the Supporting Information. The eigenvector in the TS corresponding to the imaginary frequency is primarily a motion of the reactive hydrogen atom being transferred between the C_1 and the O_1 centers for the (1,3s) isomerization, and between the C_4 and the O_1 centers for the (1,6p) isomerization. Vibrational frequencies have been scaled using appropriate scaling factors[48] for the computation of the partition functions as a function of the temperature (0.970 and 0.952 for B3LYP/cc-pVDZ and MPW1K/6-31+G(d,p), respectively).

2. Energetics. Table 3 lists the reaction enthalpies ($\Delta_r H$) computed at 0 K. The results obtained with the MPW1K method indicate that the reaction is predicted to be endothermic for both (1,3s) and (1,6p) isomerization channels. The calculated reaction enthalpies at 0 K for 2-, 3-, and 4-methylbenzylperoxy radicals (1,3s) isomerizations are very close to the value obtained at the same level of theory for the benzylperoxy radical (1,3s) isomerization (8.7 kJ mol^{-1}). It can be noticed that the (1,6p) isomerization is far more endothermic than the (1,3s) isomerization.

Table 3 shows also the computed vibrationally adiabatic barriers, E_0, for the studied reactions. The following relation defines these barriers

$$E_0 = E_{TS} - E_R + ZPE_{TS} - ZPE_R \qquad \text{(III-1)}$$

TABLE 3: Reaction Enthalpies $\Delta_r H$ at 0 K and Vibrationally Adiabatic Barriers E_0 Calculated at Different Levels of Theory

	$\Delta_r H$ (kJ mol^{-1})		E_0 (kJ mol^{-1})		
	B3LYP/cc-pVDZ	MPW1K/6-31+G(d,p)	B3LYP/cc-pVDZ	MPW1K/6-31+G(d,p)	CASPT2/ANO-L-VDZP//B3LYP/cc-pVDZ
2-methylbenzylperoxy (1,3s) isomerization	−	8.9	157.2	174.7	146.1
2-methylbenzylperoxy (1,6p) isomerization	33.9	26.3	90.4	109.3	94.6
3-methylbenzylperoxy (1,3s) isomerization	−	9.1	154.6	173.6	134.4
4-methylbenzylperoxy (1,3s) isomerization	−	9.9	154.4	173.5	137.3

where E_{TS} and E_R are the computed energies of the TS and reactant, whereas ZPE_{TS} and ZPE_R are their corresponding zero-point energy corrections.

The (1,3s) isomerization appears to have a large electronic barrier by comparison to the (1,6p) isomerization. The E_0 values calculated with the B3LYP density functional are systematically lower by about 20 kJ mol^{-1} when compared to those obtained with the MPW1K density functional. Similar results are observed with the CASPT2 method, although the barriers are lower by about 15−40 kJ mol^{-1} compared to those calculated with the B3LYP and MPW1K methods. The barriers computed with both density functionals depend slightly on the position of the methyl group on the aromatic ring and are very close to the ones obtained for the benzylperoxy radical (1,3s) isomerization[2] (155.6 and 174.7 kJ mol^{-1} at the B3LYP/cc-pVDZ and MPW1K/6-31+G(d,p) levels of theory, respectively). For the butylperoxy and pentylperoxy radicals (1,6p) isomerizations, the barriers calculated by Jungkamp et al.[27] at the CBS-lq//B3LYP/6-31G(d,p) level, Zhu et al.[24] at the CBS-QB3 level, and Chan et al.[20] at the BHandHLYP/6-311G(d,p) level were 106.3, 94.6, and 125.1 kJ mol^{-1}, respectively. Our calculated barriers with B3LYP and MPW1K density functionals for the 2-methylbenzylperoxy radical (1,6p) isomerization are close to those reported for alkylperoxy radicals. Using the CASPT2 method, the barrier calculated for the 2-methylbenzylperoxy radical (1,3s) isomerization is higher by about 9−12 kJ mol^{-1} than the ones computed for the 3- and 4-methylbenzylperoxy radical (1,3s) isomerization.

3. Kinetic Parameters Calculations. ***Rate Constants.*** Table 4 and Figure 2 present the calculated high-pressure limit rate constants over the temperature range 600−2000 K at the CASPT2/ANO-L-VDZP//B3LYP/cc-pVDZ level of theory. At 600 K, the rate constants obtained for the 3- and 4-methylbenzylperoxy (1,3s) isomerizations are only higher by a factor of about 2 than the values of the 2-methylbenzylperoxy (1,3s) isomerization. The opposite trend is observed at 2000 K while, at a temperature of about 1000 K, all the computed rate constants are very close to each other. These reactivity trends can be attributed to the small changes of the Arrhenius parameters over the studied temperature range (see section below). Using the Arrhenius parameters, which are gathered in Table 5, one can compute the rate constants at 773 K. We obtain respectively 1.8×10^3, 2.4×10^3, and 2.4×10^3 s^{-1} for the 2-, 3-, and 4-methylbenzylperoxy (1,3s) isomerizations. These values are very close to the value calculated at the same level of theory for the benzylperoxy (1,3s) isomerization (2.5×10^3 s^{-1}).[2]

Branching Ratio. We can define the branching ratio τ_X (in percent) as the ratio of the rate constant for the X-isomerization pathway to that of the overall rate constant of the reaction. For example, in the case of the 2-methylbenzylperoxy radical, the branching ratio for the (1,3s) isomerization channel is given by the following equation

$$\tau_{(1,3s)} = \frac{k_{(1,3s)}(T)}{k_{(1,3s)}(T) + k_{(1,6p)}(T)} \times 100\% \qquad \text{(III-2)}$$

where $k_{(1,3s)}(T)$ and $k_{(1,6p)}(T)$ are the rate constants for the (1,3s) and (1,6p) isomerization channels at temperature T, respectively. The results of these calculations are summarized in graphical form in Figure 3, where the temperature dependence of the branching ratios of the two channels is depicted. The (1,6p) isomerization is consistently the most important channel over the temperature range 600−1800 K. At 1800 K, the two isomerization channels are competitive. At higher temperature, the (1,3s) isomerization becomes the most important channel. Nevertheless, it can be noticed that both channels should be

TABLE 4: Calculated Rate Constants in s^{-1} over the Temperature Range 600−2000 K at the CASPT2/ANO-L-VDZP//B3LYP/cc-pVDZ Level of Theory

T (K)	2-methylbenzylperoxy (1,3s) isomerization	2-methylbenzylperoxy (1,6p) isomerization	3-methylbenzylperoxy (1,3s) isomerization	4-methylbenzylperoxy (1,3s) isomerization
600	2.02×10^0	3.16×10^3	4.93×10^0	4.13×10^0
700	1.34×10^2	4.33×10^4	2.33×10^2	2.12×10^2
800	3.18×10^3	3.14×10^5	4.27×10^3	4.15×10^3
900	3.78×10^4	1.49×10^6	4.16×10^4	4.25×10^4
1000	2.77×10^5	5.23×10^6	2.60×10^5	2.76×10^5
1100	1.42×10^6	1.47×10^7	1.17×10^6	1.29×10^6
1200	5.60×10^6	3.52×10^7	4.14×10^6	4.66×10^6
1300	1.79×10^7	7.39×10^7	1.21×10^7	1.39×10^7
1400	4.88×10^7	1.40×10^8	3.05×10^7	3.58×10^7
1500	1.17×10^8	2.45×10^8	6.81×10^8	8.12×10^8
1600	2.51×10^8	4.00×10^8	1.38×10^8	1.67×10^8
1700	4.93×10^8	6.18×10^8	2.57×10^8	3.16×10^8
1800	9.01×10^8	9.12×10^8	4.49×10^8	5.57×10^8
1900	1.55×10^9	1.29×10^9	7.39×10^8	9.27×10^8
2000	2.52×10^9	1.77×10^9	1.16×10^9	1.47×10^9

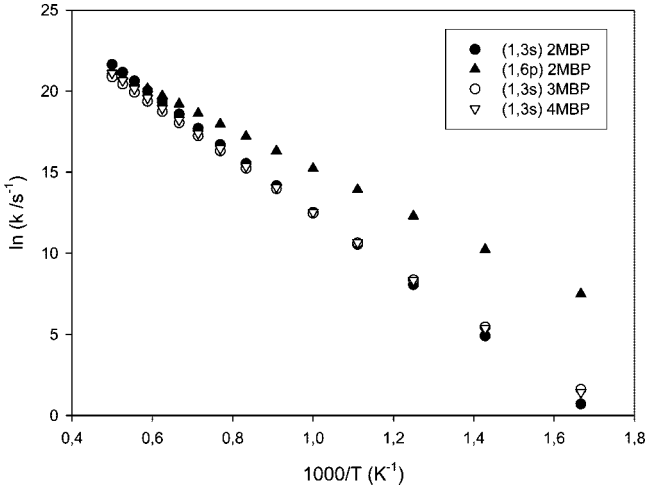

Figure 2. Evolution of ln k as a function of 1000/T for the different isomerization reactions.

TABLE 5: Summary of the Arrhenius Parameters of the Different Isomerization Reactions Calculated over the Temperature Range 600−2000 K

	A (s^{-1})	n	E_a (kJ mol^{-1})
2-methylbenzylperoxy (1,3s) isomerization	3.33×10^{10}	0.79	142.6
2-methylbenzylperoxy (1,6p) isomerization	5.10×10^{8}	0.85	87.1
3-methylbenzylperoxy (1,3s) isomerization	0.74×10^{10}	0.79	130.7
4-methylbenzylperoxy (1,3s) isomerization	1.12×10^{10}	0.79	133.6

taken into account for the calculation of the pseudoglobal rate constant (considering only the (1,3s) and (1,6p) channels) over the whole temperature range.

Other dissociation channels do exist for the methylbenzylperoxy radical such as the ones depicted by Murakami et al.[26] for the benzylperoxy radical. They are not taken into consideration here and could be studied in order to explain the fate of the methylbenzylperoxy radical under combustion conditions.

Arrhenius Parameters. The modified three-parameter Arrhenius expression, $k(T) = A \times T^n \exp(-E_a/RT)$, fitted to each elementary rate constant computed at the CASPT2/ANO-L-VDZP//B3LYP/cc-pVDZ level of theory over the temperature range 600−2000 K, is reported in Table 5. Based on our previous work on the kinetics of the benzylperoxy radical isomerization,[2] we are confident in our predicted Arrhenius parameters for the 2-, 3-, and 4-methylbenzylperoxy radicals isomerization. Therefore, these values can be recommended for use in the thermokinetic models involving aromatic compounds.

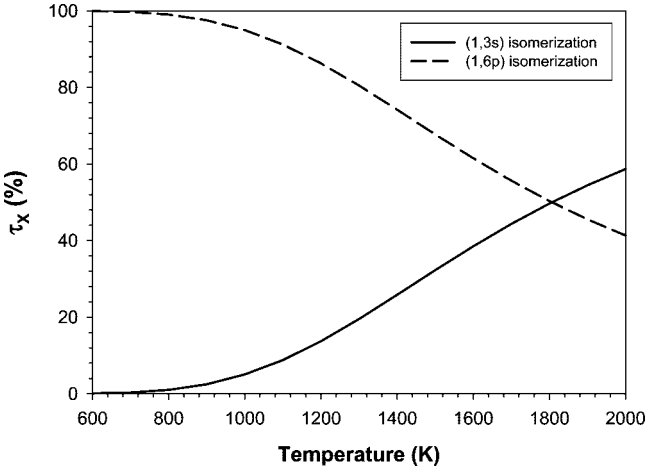

Figure 3. Temperature dependence of the branching ratio τ_x in percent of the 2-methylbenzylperoxy radical (1,3s) and (1,6p) isomerizations.

Conclusion

Theoretical calculations combined with canonical TST were performed on the reaction of the four-center and seven-center isomerizations of the 2-, 3-, and 4-methylbenzylperoxy radicals. The geometry parameters for the reactants, the products, and the TSs were fully optimized with the B3LYP and MPW1K methods combined with the cc-pVDZ and 6-31+G(d,p) basis sets, respectively. Following our previous recommendation, the CASPT2/ANO-L-VDZP//B3LYP/cc-pVDZ level of theory was used for the calculation of the high-pressure limit rate constants over the temperature range 600−2000 K. It has been shown that, in the case of the 2-methylbenzylperoxy radical, the (1,6p) H-atom transfer reaction is consistently the most important channel over the studied temperature range. As previously discussed in the Introduction, two internal H-atom transfer reactions of 2-methylbenzylperoxy radical were considered to explain the observed oxidation products. In particular, the (1,3s) H-atom transfer reaction was used to explain the *o*-tolualdehyde formation. In the light of our calculations, this reaction pathway is not energetically favored. Another mechanism leading to *o*-tolualdehyde should be considered to explain its formation.

Acknowledgment. We thank the Institut du Développement et des Ressources en Informatique Scientifique, the Centre de Ressources Informatiques de HAute Normandie, and the Centre de Ressources Informatiques of the University of Lille 1 for providing computing time for part of the theoretical calculations. We thank the Nord Pas de Calais Region, the European funds for Regional Economic Development, and the Air Quality Program of the Institut de Recherche en ENvironnment Industriel for their financial support.

Supporting Information Available: Optimized geometry parameters and vibrational frequencies for the reactants, the products, and the different transition states. This material is available free of charge via the Internet at http://pubs.acs.org.

References and Notes

(1) Walker, R. W., Morley, C. In *Low-Temperature Combustion and Autoignition*, Chapter 1; Compton, R. G., Hancock, G., Eds.; Comprehensive Chemical Kinetics Series; Elsevier Science: Amsterdam, The Netherlands, 1997; Vol. 35, pp 1−124.

(2) Canneaux, S.; Louis, F.; Ribaucour, M.; Minetti, R.; El Bakali, A.; Pauwels, J.-F. *J. Phys. Chem. A* **2008**, *112*, 6045–6052.

(3) Ellis, C. M.; Scott, S.; Walker, R. W. *Combust. Flame* **2003**, *132*, 291–304.

(4) El Bakali, A.; Ribaucour, M.; Saylam, A.; Vanhove, G.; Therssen, E.; Pauwels, J.-F. *Fuel* **2006**, *85*, 881–895.

(5) Guibet, J.-C. *Carburants et moteurs Technologies−Energie−Environnement*; Editions Technip: Paris, 1997; Vol. 1, pp 55−61.

(6) Guibet, J.-C. *Carburants et moteurs Technologies−Energie−Environnement*; Editions Technip: Paris, 1997; Vol. 1, p 239.

(7) Salooja, K. C. In *Motor Gasolin*; Marshall, E. L., Owen, K., Eds.; Special Report on Applied Chemistry; The Royal Society of Chemistry: Cambridge, U.K., 1995; Vol. 34, p 4.

(8) Emdee, J. L.; Brezinsky, K.; Glassman, I. *Symp. (Int.) Combust., [Proc.]* **1990**, *23*, 77–84.

(9) Emdee, J. L.; Brezinsky, K.; Glassman, I. *J. Phys. Chem.* **1991**, *95*, 1626–1635.

(10) Gregory, D.; Jackson, R. A. *Combust. Flame* **1999**, *118*, 459–468.

(11) Dupont, L. Etudes expérimentales et modélisation cinétique de la dégradation thermique des composés organiques volatils aromatiques

benzène, toluène et *para*-xylène dans des flammes de méthane. Ph.D. Thesis, Université des Sciences et Technologies de Lille, Villeneuve d'Ascq, France, February 16, 2001.

(12) Gaïl, S. Étude cinétique de l'oxydation de composés aromatiques en relation avec la combustion du gazole et de l'essence: approche expérimentale et modélisation cinétique détaillée. Ph.D. Thesis, Université d'Orléans, Orléans, France, November 27, 2003.

(13) Gaïl, S.; Dagaut, P. *Combust. Flame* **2005**, *141*, 281–297.

(14) Battin-Leclerc, F.; Bounaceur, R.; Belmekki, N.; Glaude, P. A. *Int. J. Chem. Kinet.* **2006**, *38*, 284–302.

(15) Loftus, J.; Satterfield, C. N. *J. Phys. Chem.* **1965**, *69*, 909–918.

(16) Barnard, J. A.; Sankey, B. M. *Combust. Flame* **1968**, *12*, 345–352.

(17) Barnard, J. A.; Sankey, B. M. *Combust. Flame* **1968**, *12*, 353–359.

(18) Roubaud, A.; Minetti, R.; Sochet, L. R. *Combust. Flame* **2000**, *121*, 535–541.

(19) Roubaud, A.; Lemaire, O.; Minetti, R.; Sochet, L. R. *Combust. Flame* **2000**, *123*, 561–571.

(20) Chan, W.-T.; Hamilton, I. P.; Pritchard, H. O. *J. Chem. Soc., Faraday Trans.* **1998**, *94*, 2303–2306.

(21) Sheng, C. Y.; Bozzelli, J. W.; Dean, A. M.; Chang, A. Y. *J. Phys. Chem. A* **2002**, *106*, 7276–7293.

(22) Sun, H.; Bozzelli, J. W. *J. Phys. Chem. A* **2004**, *108*, 1694–1711.

(23) Lee, J.; Bozzelli, J. W. *Proc. Combust. Inst.* **2005**, *30*, 1015–1022.

(24) Zhu, L.; Bozzelli, J. W.; Kardos, L. M. *J. Phys. Chem. A* **2007**, *111*, 6361–6377.

(25) Clothier, P. Q. E.; Shen, D.; Pritchard, H. O. *Combust. Flame* **1995**, *101*, 383–386.

(26) Murakami, Y.; Oguchi, T.; Hashimoto, K.; Nosaka, Y. *J. Phys. Chem. A* **2007**, *111*, 13200–13208.

(27) Jungkamp, T. P. W.; Smith, J. N.; Seinfeld, J. H. *J. Phys. Chem. A* **1997**, *101*, 4392–4401.

(28) Frisch, M. J.; Trucks, G. W.; Schlegel, H. B.; Scuseria, G. E.; Robb, M. A.; Cheeseman, J. R.; Montgomery, J. A., Jr.; Vreven, T.; Kudin, K. N.; Burant, J. C.; Millam, J. M.; Iyengar, S. S.; Tomasi, J.; Barone, V.; Mennucci, B.; Cossi, M.; Scalmani, G.; Rega, N.; Petersson, G. A.; Nakatsuji, H.; Hada, M.; Ehara, M.; Toyota, K.; Fukuda, R.; Hasegawa, J.; Ishida, M.; Nakajima, T.; Honda, Y.; Kitao, O.; Nakai, H.; Klene, M.; Li, X.; Knox, J. E.; Hratchian, H. P.; Cross, J. B.; Bakken, V.; Adamo, C.; Jaramillo, J.; Gomperts, R.; Stratmann, R. E.; Yazyev, O.; Austin; A. J.; Cammi, R.; Pomelli, C.; Ochterski, J. W.; Ayala, P. Y.; Morokuma, K.; Voth, G. A.; Salvador, P.; Dannenberg, J. J.; Zakrzewski, V. G.; Dapprich, S.; Daniels, A. D.; Strain, M. C.; Farkas, O.; Malick, D. K.; Rabuck, A. D.; Raghavachari, K.; Foresman, J. B.; Ortiz, J. V.; Cui, Q.; Baboul, A. G.; Clifford, S.; Cioslowski, J.; Stefanov, B. B.; Liu, G.; Liashenko, A.; Piskorz, P.; Komaromi, I.; Martin, R. L.; Fox, D. J.; Keith, T.; Al-Laham, M. A.; Peng, C. Y.; Nanayakkara, A.; Challacombe, M.; Gill, P. M. W.; Johnson, B.; Chen, W.; Wong, M. W.; Gonzalez, C.; Pople, J. A. *GAUSSIAN 03*, Revision D.01; Gaussian, Inc.: Wallingford CT, 2004.

(29) Karlström, G.; Lindh, R.; Malmqvist, P.-A.; Roos, B. O.; Ryde, U.; Veryazov, V.; Widmark, P.-O.; Cossi, M.; Schimmelpfennig, B.; Neogrady, P.; Seijo, L. *Comput. Mater. Sci.* **2003**, *28*, 222–239.

(30) Lee, C.; Yang, W.; Parr, R. *Phys. Rev. B* **1988**, *37*, 785–789.

(31) Becke, A. *J. Chem. Phys.* **1993**, *98*, 5648–5652.

(32) Lynch, B. J.; Fast, P. L.; Harris, M.; Truhlar, D. G. *J. Phys. Chem. A* **2000**, *104*, 4811–4815.

(33) Descriptions of the Pople-style basis sets can be found in: Foresman, J. B.; Frisch, A. E. *Exploring Chemistry with Electronic Structure Methods*, 2nd ed.; Gaussian, Inc.: Pittsburgh, PA, 1996.

(34) (a) Dunning, T. H., Jr. *J. Chem. Phys.* **1989**, *90*, 1007–1023. (b) Woon, D. E.; Dunning, T. H., Jr. *J. Chem. Phys.* **1993**, *98*, 1358–1371. (c) Woon, D. E.; Dunning, T. H., Jr. *J. Chem. Phys.* **1994**, *100*, 2975–2988. (d) Wilson, A. K.; Woon, D. E.; Peterson, K. A.; Dunning, T. H., Jr. *J. Chem. Phys.* **1999**, *110*, 7667–7676.

(35) Gonzalez, C.; Schlegel, H. B. *J. Chem. Phys.* **1989**, *90*, 2154–2161.

(36) Roos, B. O.; Andersson, K.; Fulscher, M. P.; Malmqvist, P.-A.; Serrano-Andres, L.; Pierloot, K.; Merchan, M. *Advances in Chemical Physics*; Wiley & Sons: New York, 1996; Vol. XCIII.

(37) Andersson, K. In *Encyclopedia of Computational Chemistry*; Wiley: New York, 1998; p 460.

(38) Andersson, K.; Malmqvist, P.-A.; Roos, B. O.; Sadlej, A. J.; Wolinski, K. *J. Phys. Chem.* **1990**, *94*, 5483–5488.

(39) Andersson, K.; Malmqvist, P.-A.; Roos, B. O. *J. Chem. Phys.* **1992**, *96*, 1218–1226.

(40) Widmark, P.-O.; Malmqvist, P.-A.; Roos, B. O. *Theor. Chim. Acta* **1990**, *77*, 291–306.

(41) (a) Eyring, H. *J. Chem. Phys.* **1935**, *3*, 107–115. (b) Johnston, H. S. *Gas Phase Reaction Rate Theory*; The Roland Press Co.: New York, 1966. (c) Laidler, K. J. *Theories of Chemical Reaction Rates*; McGraw-Hill: New York, 1969. (d) Weston, R. E.; Schwartz, H. A. *Chemical Kinetics*; Prentice-Hall: New York, 1972. (e) Rapp, D. *Statistical Mechanics*; Holt, Reinhard, and Winston: New York, 1972. (f) Nikitin, E. E. *Theory of Elementary Atomic and Molecular Processes in Gases*; Claredon Press: Oxford, 1974. (g) Smith, I. W. M. *Kinetics and Dynamics of Elementary Gas Reactions*; Butterworths: London, 1980. (h) Steinfeld, J. I.; Francisco, J. S.; Hase, W. L. *Chemical Kinetics and Dynamics*; Prentice-Hall: Englewood Cliffs, NJ, 1989.

(42) Wigner, E. P. *Z. Phys. Chem.* **1932**, *B19*, 203–216.

(43) (a) Bell, R. P. *The Tunnel Effect in Chemistry*; Chapman and Hall: New York, 1980. (b) Louis, F.; Gonzalez, C.; Sawerysyn, J.-P. *J. Phys. Chem. A* **2004**, *108*, 10586–10593.

(44) (a) Garrett, B. C.; Truhlar, D. G. *J. Phys. Chem.* **1979**, *83*, 2921–2926. (b) Garrett, B. C.; Truhlar, D. G. *J. Chem. Phys.* **1984**, *81*, 309–317. (c) Skodje, R. T.; Garrett, B. C.; Truhlar, D. G. *J. Phys. Chem.* **1981**, *85*, 3019–3023. (d) Skodje, R. T.; Garrett, B. C.; Truhlar, D. G. *J. Chem. Phys.* **1982**, *77*, 5955–5976. (e) Garrett, B. C.; Truhlar, D. G.; Grev, R. S.; Magnuson, A. W. *J. Phys. Chem.* **1980**, *84*, 1730–1748. (f) Garrett, B. C.; Truhlar, D. G.; Grev, R. S.; Magnuson, A. W. *J. Phys. Chem.* **1983**, *87*, 4554–4554.

(45) (a) Miller, W. H.; Shi, S.-H. *J. Chem. Phys.* **1981**, *75*, 2258–2264. (b) Miller, W. H.; Smith, F. T. *Phys. Rev.* **1978**, *A17*, 939–953.

(46) Henon, E.; Bohr, F.; Canneaux, S.; Postat, B.; Auge, F.; Bouillard, E.; Domureau, V. *KISTHEP 1.0*; University of Reims Champagne-Ardenne: France, 2003.

(47) Garcia, I.; Ruiz, M. E.; Smeyers, Y. G.; Vivier Bunge, A. *J. Mol. Struct.: THEOCHEM* **1995**, *340*, 149–158.

(48) NIST Computational Chemistry Comparison and Benchmark Database; Johnson, R. D., III., Ed.; NIST Standard Reference Database Number 101 Release 14, Sept. 2006;http://srdata.nist.gov/cccbdb.

JP811137D